Dispersion and Attenuation Characteristics of Coplanar Waveguides with Finite Metallization Thickness and Conductivity

Jeng-Yi Ke and Chun Hsiung Chen

Abstract—**A new approach of modifying the conventional spectral-domain approach is proposed for an analysis of the coplanar waveguide whose signal strip and ground planes have finite thickness and conductivity. By introducing suitable equivalent sources in the slot and signal strip regions, the problem can be significantly simplified by reducing the two-dimensional numerical integration into the one-dimensional one, thus it can be treated as easily as the conventional spectral-domain approach. By this modified approach, both the phase constant and attenuation constant can be determined simultaneously without using the assumption that the metallization thickness is much larger or smaller than the skin depth. In this work, comparison with published theoretical and experimental results is presented to check the accuracy of the new approach's results. In particular, the effective dielectric constant ϵ_{eff} and attenuation constant α of a coplanar waveguide with finite metallization thickness and finite conductivity are discussed in detail, together with the current distributions along the signal strip and ground planes.**

I. Introduction

THE COPLANAR waveguide structure has become an intensive topic of current research due to some of its attractive characteristics with respect to those of the microstrip line. One advantage is the easy connection of both series and shunt components without drilling holes through the dielectric substrate. The substrate need not be made very thin in millimeter-wave region, offering more parameters for characteristics adjustment. It is also less dispersive than the microstrip line, making the quasi-static design formulas applicable to the higher frequency regime.

Previous analysis of coplanar waveguides was usually conducted under the assumptions of infinitely thin conductors and infinite conductivity. Recently, the problem of finite metallization thickness and finite conductivity has received increased attention, because the conductor thickness may be comparable to the skin depth in monolithic microwave integrated circuits (MMIC's). With the metallization thickness in the order of skin depth, the propagation characteristics, especially the attenuation constant, would behave different from the previous ones of assuming zero metallization thickness or assuming infinite conductivity but with finite metallization thickness [1]. Thus, a more reliable and accurate model to determine the propagation constant is needed in the design of monolithic microwave and millimeter-wave integrated circuits [2].

The characterization of attenuation by the conventional power-loss method [3] or Wheeler's incremental inductance rule [4] becomes inadequate in a design of MMIC's because it was based on the skin-depth approximation that the metallization thickness is much larger than the skin depth. Recently, some full-wave approaches such as the transverse resonance technique [5] and the extended spectral domain approach [6]–[7] were proposed to deal with the problem of finite metallization thickness and finite conductivity. In these approaches, the conductivity was first regarded as infinity to get the effective dielectric constant and the fields, and then used these unperturbed fields and the power-loss method to determine the loss caused by the imperfect conductors. Other full-wave techniques without using the skin-depth approximation, such as mode matching method [8], [9] and method of lines [10], were also proposed to give a better characterization of both effective dielectric constant and attenuation constant. However, these techniques can only handle the bounded structures. Therefore, an effective method with less assumptions to get the propagation constant is needed to meet the development of mm-wave technology.

For an analysis of the coplanar waveguide with layer structure in which the thickness and conductivity of conductors are finite, a new formulation of modifying the conventional spectral-domain approach is proposed to handle the case with two-dimensional dependence in field distributions. In this formulation, the only unknown is the electric field confined to the slot and signal strip regions. To improve the accuracy in computation all three components of electric field are included, and the effects of lossy signal strip and ground planes are discussed. And by this modification, the integration along one coordinate variable is analytically integrated. Hence it is as easy as the conventional spectral-domain approach in which only one-dimensional integration has to be performed to get the matrix equation for the propagation constant. To reduce the CPU time, an alternative representation of the unknown field by some already calculated better field distributions is also proposed [11] when the metallization thickness is much larger than the skip depth.

II. Formulation

The cross-section of the coplanar waveguide is shown in Fig. 1(a). Here, t is the thickness of the signal strip and the

Manuscript received June 21, 1994; revised September 12, 1994. This work was supported by the National Science Council of Taiwan, R.O.C. under Grant NSC 83-0404-E-002-044.

The authors are with the Department of Electrical Engineering, National Taiwan University, Taipei, Taiwan 10617, R.O.C.

IEEE Log Number 9410338.

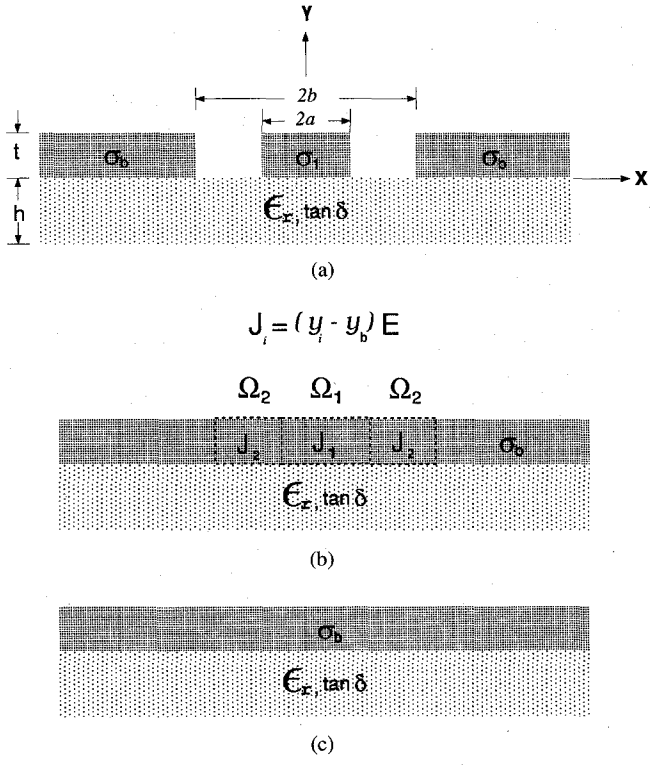

Fig. 1. (a) Cross-section of coplanar waveguide, (b) equivalence problem in formulation, and (c) layer structure for deriving Green's functions.

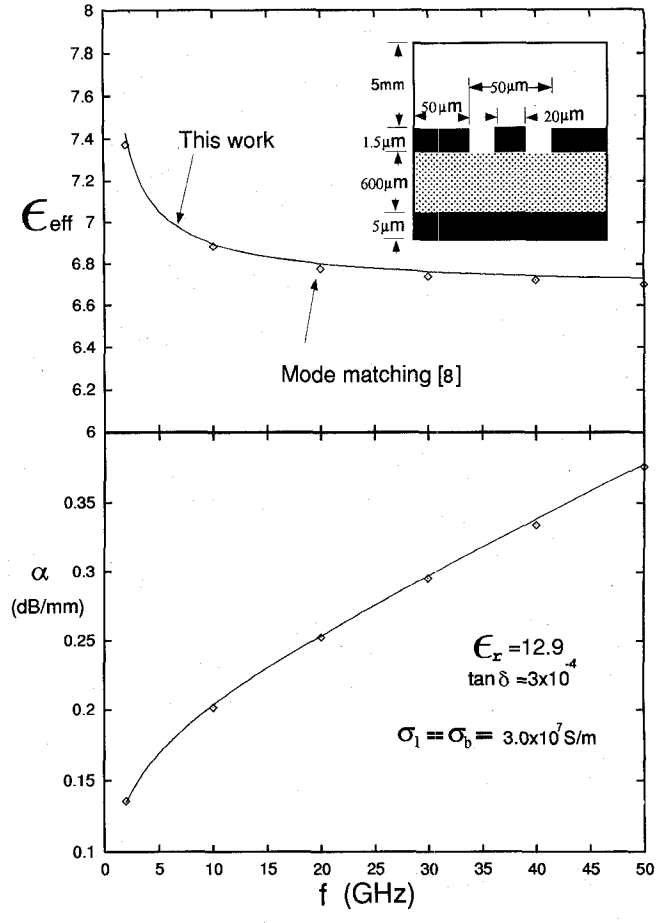

Fig. 2. Comparison of effective dielectric constant ϵ_{eff} and attenuation constant α with those of mode matching technique.

ground planes, σ_1 is the conductivity of signal strip, and σ_b is the conductivity of the ground planes. The width of the signal strip is $2a$, the distance between the ground planes is $2b$; and the thickness, dielectric constant, and loss tangent of the substrate are h, ϵ_r, and $\tan\,\delta$, respectively. To solve this problem, the equivalent structure shown in Fig. 1(b) is investigated. In this equivalent problem, the signal strip and the slots are replaced by the conductor of conductivity σ_b, and the equivalent currents $\mathbf{J}_1 = (y_1 - y_b)\mathbf{E}$ and $\mathbf{J}_2 = (y_2 - y_b)\mathbf{E}$ are introduced in the signal strip region Ω_1 and slot region Ω_2, respectively, where $y_1 = j\omega\epsilon_0 + \sigma_1, y_2 = j\omega\epsilon_0$, and $y_b = j\omega\epsilon_0 + \sigma_b$. The relation between the electric field $\mathbf{E}(\mathbf{r})$ and the equivalent current densities $\mathbf{J}_i(\mathbf{r})$ within the signal strip and slot regions is

$$\mathbf{E}(\mathbf{r}) = \sum_{i=1}^{2} (y_i - y_b) \int_{\Omega_i} \overline{\overline{\mathbf{G}}}(r - r') \cdot \mathbf{E}(\mathbf{r}')\, d\mathbf{r}'. \quad (1)$$

Here, $\overline{\overline{\mathbf{G}}}$ is the dyadic Green's function for the layer structure as shown in Fig. 1(c). It should be emphasized that the conductors are now regarded as a lossy layer therefore the effect of lossy signal strip and ground planes may be discussed through these Green's functions. Some detail of the Green functions is presented in the Appendix.

For the important special case of $\sigma_1 = \sigma_b$ in which both signal strip and ground planes have same conductivities, the equivalent current $\mathbf{J}_1$ in the strip region Ω_1 is zero, thus the integral equation (1) need only be solved in the slot region Ω_2.

All field quantities are assumed to be of the form $\exp[j(\omega t - k_z z)]$, and the Fourier transformation pair is defined as

$$\tilde{A}(k_x) = \int_{-\infty}^{\infty} A(x) e^{-jk_x x}\, dx$$
$$A(x) = \frac{1}{2\pi} \int_{-\infty}^{\infty} \tilde{A}(k_x) e^{jk_x x}\, dk_x. \quad (2)$$

By weighting both sides of (1) by any arbitrary function $\mathbf{w}(\mathbf{r})$ and then integrated, one may get the integral equation

$$\int_{-b}^{b}\int_{0}^{t} \mathbf{w}(x,y) \cdot \left\{ \sum_{i=1}^{2} (y_i - y_b) \int_{-b}^{b}\int_{0}^{t} \overline{\overline{\mathbf{G}}}(x,y,x',y',k_z) \cdot \mathbf{E}(x',y')\, dy'\, dx' - \mathbf{E}(x,y) \right\} dy\, dx = 0. \quad (3)$$

It is interesting to note that the y-dependence form of the spectral-domain Green functions is a linear combination of $\exp(j\beta_b y)$ and $\exp(j\beta_b y')$, where β_b is independent of y or y' (see Appendix). Thus, if the bases of $\mathbf{E}(x,y)$ are properly chosen, the integral equation (3) can be significantly simplified.

With the parameters (t, σ_1, σ_b) of signal strip and ground planes absorbed in the Green's functions, the only unknowns

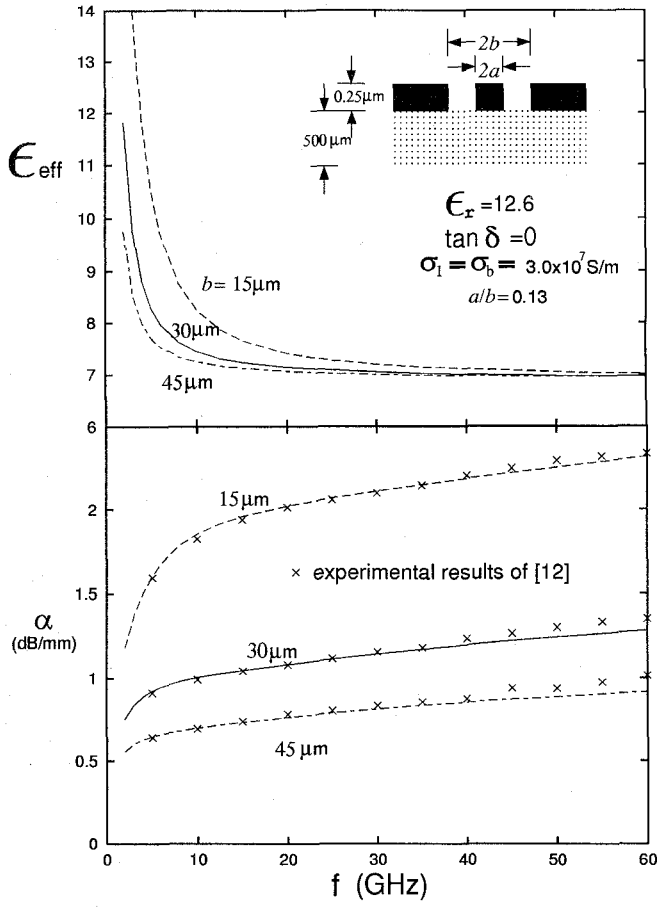

Fig. 3. Effective dielectric constant ϵ_{eff} and attenuation constant α versus frequency with aperture width b as parameters.

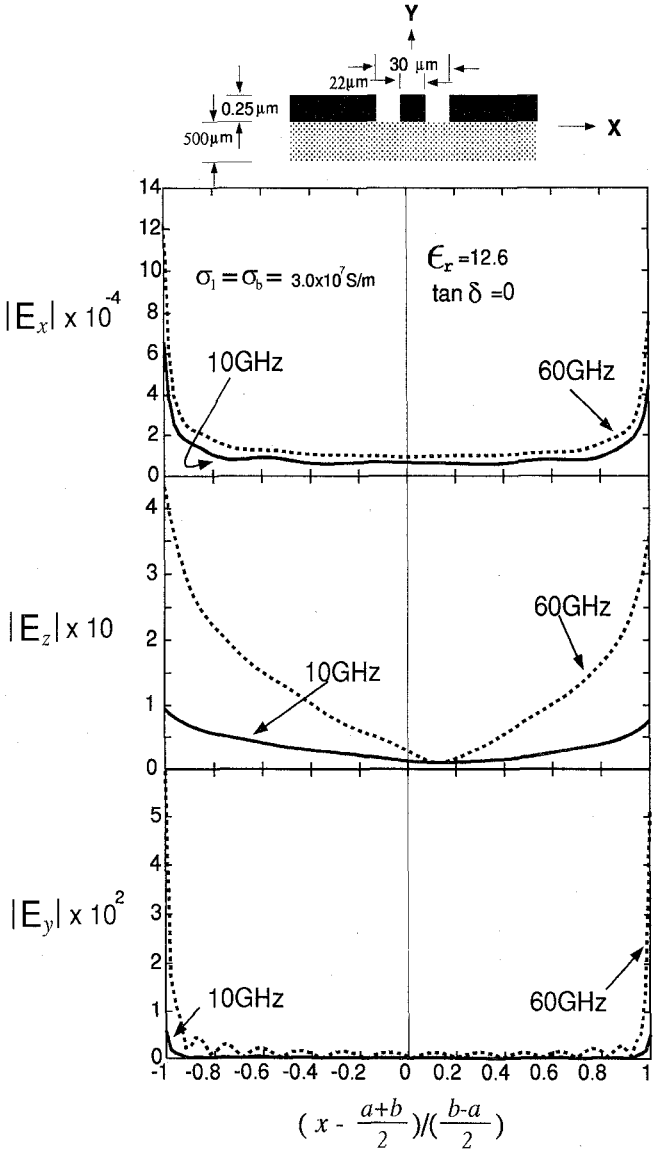

Fig. 4. Typical field distributions in slot region.

are the electric field distributions within the slot and signal strip regions which can be represented by

$$E_p(x,y) = \sum_{i=0}^{m}\sum_{j=0}^{n} a_p^{ij}\psi_p^i(x)\phi_p^j(y), \quad p = x,y,z \qquad (4)$$

where $\psi_p^l(x)$ is the Legendre polynomial and $\phi_p^l(y)$ is the piecewise linear function. Here $(m+1)$ x-dependent and $(n+1)$ y-dependent bases are included in the approximation of the unknown fields in the slot and strip regions. It should be pointed out that to get a more accurate result for the propagation constant, all three components of electric field should be included in the analysis. By applying the Fourier transformation and Parseval's theorem with respect to x variable to (3), then analytically integrating it with respect to y variable, one may finally yield the governing equations in the spectral domain. Note that only single integration with respect to k_x is involved in the final spectral-domain equations, since the y-dependent integrations have been analytically integrated. Thus, it can use the conventional technique of spectral-domain approach to find the phase and attenuation constants.

Because the thickness t and conductivities (σ_1, σ_b) are finite, the field distributions within the slot and strip regions must be finite. In this study, the Legendre polynomials are chosen as the x-dependent bases for the unknown field distributions $\mathbf{E}$, that is,

$$\psi_z^l(x) = \psi_y^l(x) = \begin{cases} P_{2l}\left(\dfrac{x}{a}\right), & |x| < a \\ P_l\left(\dfrac{x - \frac{a+b}{2}}{\frac{b-a}{2}}\right) + (-1)^l P_l\left(\dfrac{x + \frac{a+b}{2}}{\frac{b-a}{2}}\right), & a < |x| < b \end{cases}$$

$$\psi_x^l(x) = \begin{cases} P_{2l+1}\left(\dfrac{x}{a}\right), & |x| < a \\ P_l\left(\dfrac{x - \frac{a+b}{2}}{\frac{b-a}{2}}\right) + (-1)^{l+1} P_l\left(\dfrac{x + \frac{a+b}{2}}{\frac{b-a}{2}}\right), & a < |x| < b. \end{cases} \qquad (5)$$

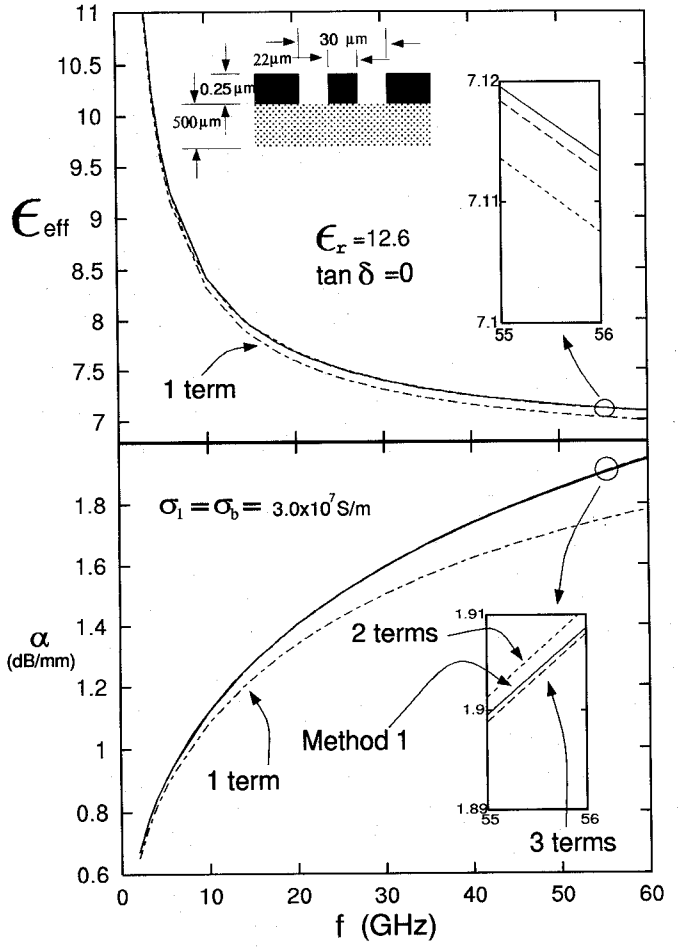

Fig. 5. Convergence of method 2 with reference to method 1.

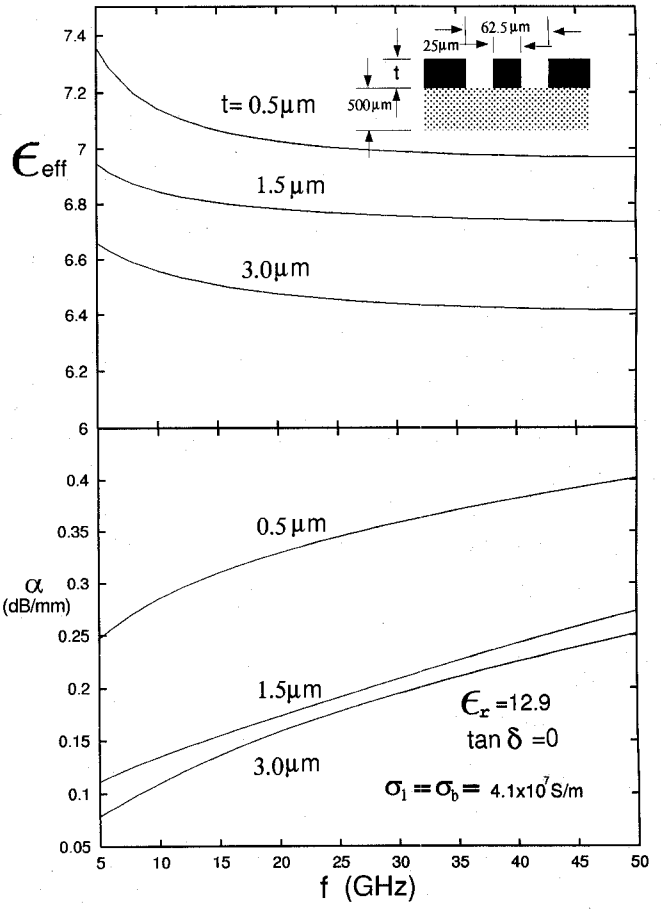

Fig. 6. Effective dielectric constant ϵ_{eff} and attenuation constant α versus frequency with metallization thickness t as parameters.

For simplicity, the following piecewise linear functions will be chosen as the y-dependent bases for the unknown field $\mathbf{E}$

$$\phi_z^l(y) = \phi_x^l(y) = \phi_y^l(y) = \wedge(y) = \begin{cases} \dfrac{y - \Delta_{l-1}}{\Delta}, & \Delta_{l-1} < y < \Delta_l \\ \dfrac{\Delta_{l+1} - y}{\Delta}, & \Delta_l < y < \Delta_{l+1} \\ 0, & \text{otherwise} \end{cases} \tag{6}$$

where $\Delta_l = l\Delta$ and $\Delta = t/n$. The piecewise linear functions are chosen for the purpose that the y-dependent integrations may be analytically integrated.

To derive the matrix equation for the propagation constant, the Galerkin's method is used, in which the bases for $\mathbf{w}(x, y)$ are the same as those for $\mathbf{E}(x, y)$. Then the propagation constant $k_z = \beta - j\alpha$ can be found by solving the homogeneous matrix equation.

III. Numerical Results

Numerical results such as effective dielectric constant $\epsilon_{eff} = \beta^2/k_0^2 (k_0^2 = \omega^2\mu_0\epsilon_0)$, attenuation constant α, and longitudinal current distributions J_z over signal strip and ground planes are investigated in detail.

To illustrate the convergence behavior with respect to the expansion in (4), a typical example with $t = 0.25\,\mu$m, $b = 15\,\mu$m, $a/b = 0.13$, $\sigma_1 = \sigma_b = 3 \times 10^7$ S/m, $\epsilon_r = 12.6$, and $\tan\delta = 0$ is considered. At 10 GHz, all three field components need 5 Legendre polynomials, and 4 piecewise linear functions to get convergent results for ϵ_{eff} and α with error less than 1%. As frequency increases to 60 GHz, 8 Legendre polynomials and 6 piecewise linear functions are required to get the same accuracy.

To check the accuracy of the new approach's results, a comparison of our results with those of the mode-matching technique [8] is presented in Fig. 2. Agreement in both effective dielectric constants ϵ_{eff} and attenuation constants α of a bounded coplanar waveguide is observed.

Shown in Fig. 3 is the effect of increasing aperture width b. Also included in this figure are the experimental results of [12]. Good agreement among these results is observed. Note that both the effective dielectric constant and attenuation constant decrease as the aperture width increases. Especially, as frequency grows, the difference in the effective dielectric constants decreases. However, the variation in attenuation by changing b is rather obvious.

As frequency increases, the thickness-to-skin depth ratio t/δ increases, making the number of bases in (4) increases. Because the CPU time is directly proportional to the square of the basis terms used, it will increase the computing time in higher frequency. To reduce the CPU time, we alternatively use the better field distributions to represent the unknown field distribution [11].

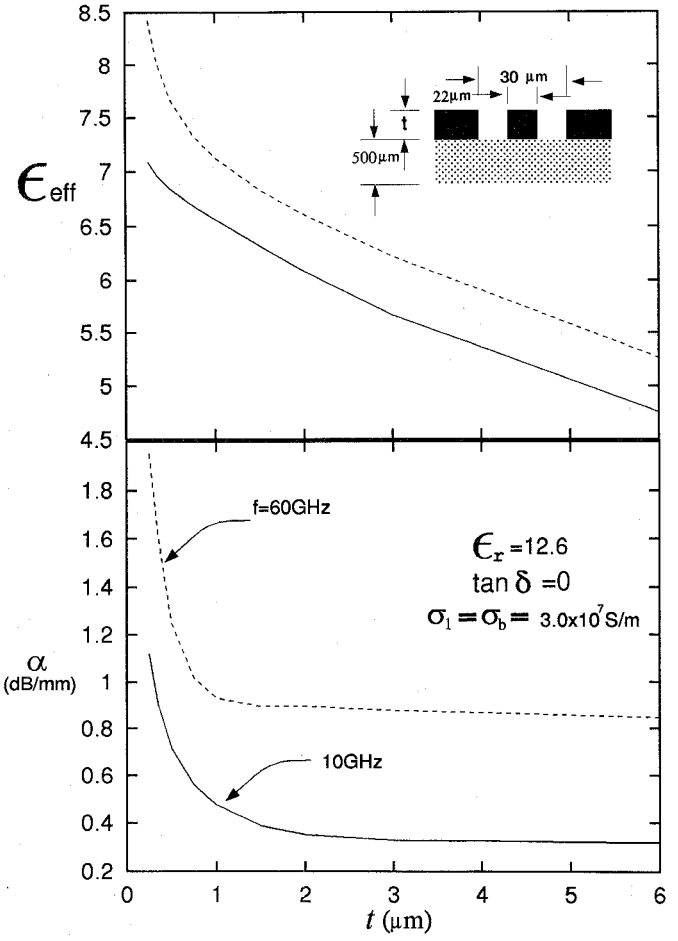

Fig. 7. Effective dielectric constant ϵ_{eff} and attenuation constant α versus t with frequency as parameters.

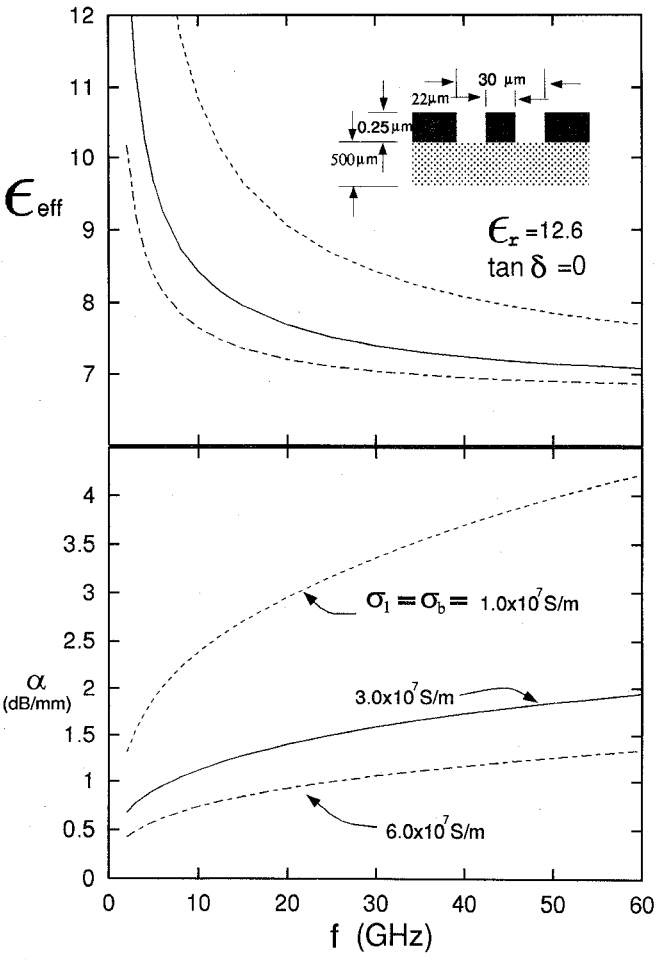

Fig. 8. Effective dielectric constant ϵ_{eff} and attenuation constant α versus frequency with conductivities $\sigma_1 (=\sigma_b)$ as parameters.

Fig. 4 shows some typical field distributions, at 10 and 60 GHz, along the air-substrate interface ($y = 0$) which are calculated by (4). One can find that, though the frequency is raised from 10 to 60 GHz, the field distributions are changed not much. This observation suggests the use of the already calculated better field distributions $\xi_p^l(x, y)$ at some specific frequency f_l by (4) to represent the unknown field distributions at other frequencies [11]

$$E_p(x, y) = \sum_{l=0}^{L} a_p^l \xi_p^l(x, y), \quad p = x, y, z. \tag{7}$$

Hereafter, we call the method by (7) as method 2, and the method by (4) as method 1.

Note that the ratio of $E_x : E_z : E_y$ in Fig. 4 is about 10^3:1:10^{-3}. Definitely, E_x is the dominant component of electric field. However, if the E_z and E_y components were omitted, the negative slope of ϵ_{eff}-curve in lower frequency would disappear and the computed attenuation constant in higher frequency would be less accurate.

Fig. 5 compares ϵ_{eff} and α calculated from these two methods. To give better results for every frequency from 10 to 60 GHz, we use 8 Legendre polynomials, and 6 piecewise linear functions in (4) to generate the curves marked "method 1." The curves marked "1 term" use the field distribution at 10 GHz by (4), the curves "2 terms" use those at 10 and 60 GHz, and the curves "3 terms" use those at 10, 20, and 60 GHz to represent the unknown field by (7). Note that the curves by method 2 converges quickly to the ones by method 1, and only two terms in (7) are required to get the desired ϵ_{eff}- and α-curves with error less than one percent. In this study, the method 2 is adopted to compute Fig. 6, and Figs. 8–10, using the field distributions at 10 and 60 GHz by method 1 to expand the unknown field distributions as given by (7).

Fig. 6 shows the effect of increasing metallization thickness t on the effective dielectric constant and attenuation constant. As expected, both the effective dielectric constant and attenuation constant decrease as t increases. It should be notes that the slope of ϵ_{eff} in low frequency range is negative. When the thickness-to-skin depth ratio t/δ approaches infinity, the current flows essentially along the conductor surface and the dispersion curve grows as the frequency increases as predicted by the conventional technique of assuming infinite conductivity. However when t and δ are of the same order, the current then penetrates into the conductor region, and this will introduce an internal inductance which then increases the effective dielectric constant in low frequency. The negative slope in ϵ_{eff}-curve is also observed theoretically [8] and experimentally [13].

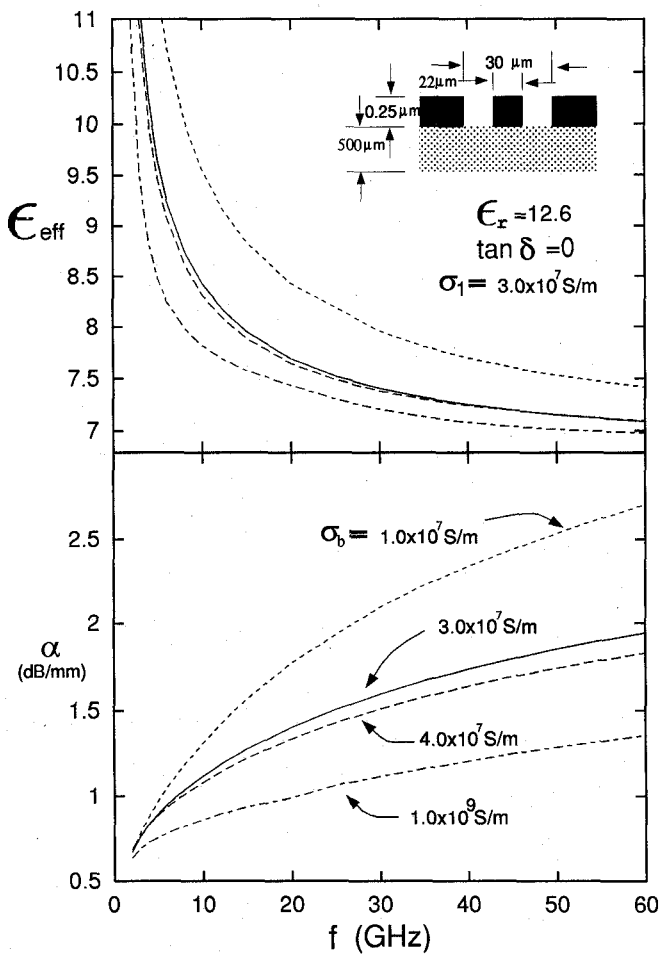

Fig. 9. Effective dielectric constant ϵ_{eff} and attenuation constant α versus frequency with conductivity of ground planes σ_b as parameters.

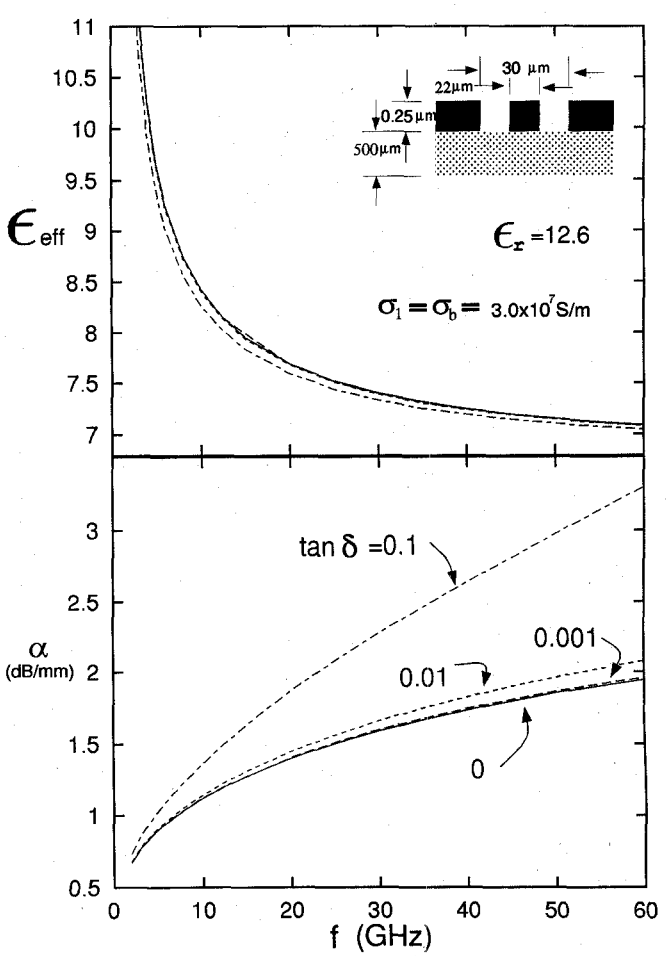

Fig. 10. Effective dielectric constant ϵ_{eff} and attenuation constant α versus frequency with substrate loss tangent $\tan\delta$ as parameters.

Fig. 7 shows the effective dielectric constant and attenuation constant vs. the thickness of signal strip and ground planes with frequency as parameters. As thickness t increases, the curves of attenuation constant decrease steeply from $t \sim 0$ to $t \sim 3\delta$ (2.7 μm for 10 GHz and 1.1 μm for 60 GHz), then change slowly, and finally approach constants. As $t > 3\delta$, the current distributes almost around the conductor surface, making the loss nearly independent of the conductor thickness. One implication is that the conductor may be regarded essentially as a perfect conductor as $t > 3\delta$, thus the simplified method, such as the extended spectral domain approach [6] or the transverse resonance technique [5] together with the perturbation approximation, may provide an efficient one of handling both the phase and attenuation constants.

The effect of increasing the conductivity $\sigma_1(=\sigma_b)$is represented in Fig. 8. Here, both the effective dielectric constant and attenuation constant decrease as σ_1 increases.

The effect of lossy ground planes is shown in Fig. 9. Both the attenuation and effective dielectric constants decrease as σ_b increases. The influence due to the finite conductivity σ_b of ground planes is smaller than that due to the conductivity σ_1 of signal strip. However when compared with the microstrip lines, the influence due to σ_b is quite large.

Shown in Fig. 10 is the effect of increasing the loss tangent $\tan\delta$. Here, the loss due to conductors are much larger than that due to substrate. However, if $\tan\delta$ is as large as 0.1, the substrate loss can be comparable with the conductor loss.

Fig. 11 shows the distribution of longitudinal current J_z on signal strip and ground planes. As expected, the edge enhancement behavior is found for the longitudinal current, but the edge current is finite instead of infinity. It is interesting to point out that the maximum ground plane current is a little smaller than the maximum signal strip current, but it decays rapidly that when $C'D'$ or $A'B'$ is equal to b, the current is about $0.2J_z(0)$. As $A'B'$ extends to $5b$, the current is about $0.005J_z(0)$. Hence to avoid the side wall effect, the dimension of the package box should be larger than $5b$.

IV. Conclusion

In this study, a modified spectral-domain approach has been proposed to deal with the coplanar waveguide with layer structure in which both the thickness and conductivity of signal strip and ground planes are finite. The effective dielectric constant ϵ_{eff} and attenuation constant α of this lossy coplanar waveguide have been discussed in detail, together with the

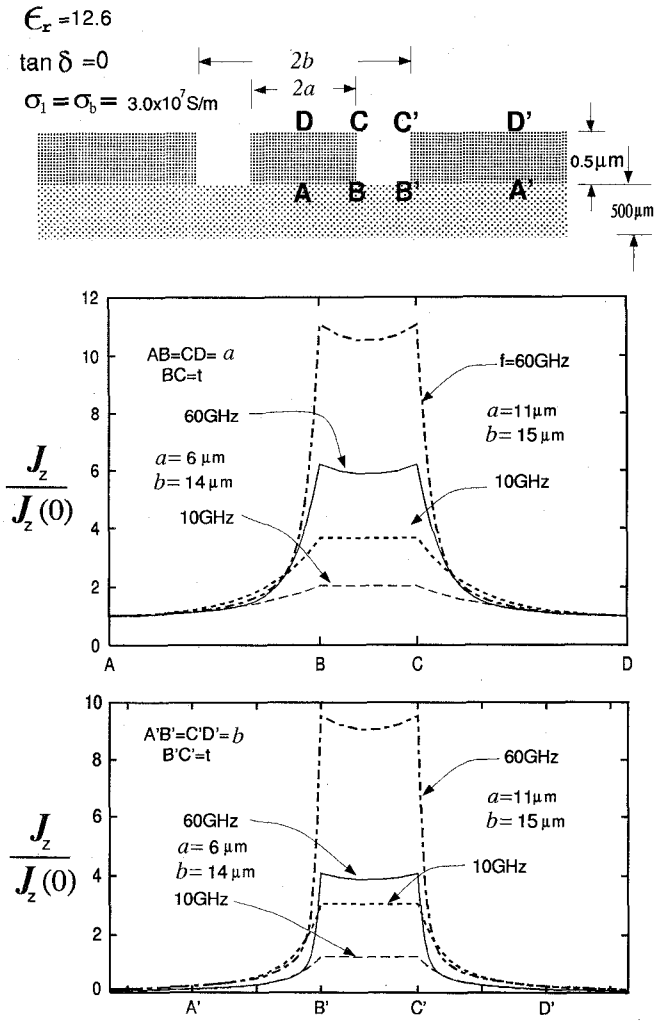

Fig. 11. Longitudinal current distributions along signal strip and ground planes.

longitudinal current distributions along the signal strip and ground planes.

The proposed approach can be applied to the structures with superconducting metallization and/or semiconductor substrates.

In this work, two methods (method 1 and method 2) are proposed to represent the unknown field distributions. The disadvantage of method 1 is that the number of bases used is proportional to the thickness-to-skin depth ratio t/δ. If the ratio t/δ is larger than 3, the computation cost will be expensive. To avoid the increased CPU time as t/δ increases, the method 2 which is based on the better field distributions calculated by method 1 should be employed.

APPENDIX

The spectral-domain dyadic Green functions $\tilde{G}_{zz}, \tilde{G}_{zx}, \tilde{G}_{xz}, \tilde{G}_{xx}, \tilde{G}_{yz}$, and $\tilde{G}_{yx}$ for the layer structure Fig. 1(c) can be developed by the method of [14], [15]. Then, the Green functions $\tilde{G}_{zy}$ and $\tilde{G}_{xy}$ can be derived from $\tilde{G}_{yz}$ and $\tilde{G}_{yx}$ by reciprocity, and the one $\tilde{G}_{yy}$ can be found easily from $\tilde{G}_{zy}$ and $\tilde{G}_{xy}$. Included here is a typical one such as

$$\tilde{G}_{xx} = \frac{-j}{2y_b(k_x^2+k_z^2)}\left(k_x^2\beta_b\Gamma_A + \frac{k_z^2k_b^2}{\beta_b}\Gamma_F\right) \tag{8}$$

where

$$\begin{aligned}\Gamma_A =& [e^{-j\beta_b|y-y'|} - \Gamma'_{A11}e^{-j\beta_b(y+y')} \\ &- \Gamma'_{A21}e^{-j\beta_b(2t-y-y')} \\ &+ \Gamma'_{A11}\Gamma'_{A21}e^{-j\beta_b(2t-|y-y'|)}] \\ &/[1-\Gamma'_{A11}\Gamma'_{A21}e^{-j\beta_b(2t)}], \\ \Gamma_F =& [e^{-j\beta_b|y-y'|} + \Gamma'_{F11}e^{-j\beta_b(y+y')} \\ &+ \Gamma'_{F21}e^{-j\beta_b(2t-y-y')} \\ &+ \Gamma'_{F11}\Gamma'_{F21}e^{-j\beta_b(2t-|y-y'|)}] \\ &/[1-\Gamma'_{F11}\Gamma'_{F21}e^{-j\beta_b(2t)}],\end{aligned}$$

and $\beta_b^2 = k_b^2 - k_x^2 - k_z^2$, $k_b^2 = y_b j\omega\mu_0$. All Γ'_{Ai1} and Γ'_{Fi1}, $(i = 1, 2)$ are defined by [15].

REFERENCES

[1] W. H. Haydl, T. Kitazawa, J. Braunstein, R. Bosch, and M. Schlechtweg, "Millimeter-wave coplanar transmission lines on gallium arsenide, indium phosphide and quartz with finite metalization thickness," in *1991 IEEE MTT-S Int. Microwave Symp. Dig.*, Boston, pp. 691–694.

[2] W. Heinrich, "Conductor loss on transmission lines in monolithic microwave and millimeter-wave integrated circuits," *Int. J. Microwave Millimeter-Wave Computer-Aided Eng.*, vol. 2, no. 3, pp. 155–167, 1992.

[3] R. E. Collin, *Field Theory of Guided Waves,* 2nd ed. New York: IEEE Press, 1991.

[4] H. A. Wheeler, "Formulas for the skin effect," *Proc. IRE,* vol. 30, pp. 412–442, 1942.

[5] F. Alessandri, G. Baini, G. D'Inzeo, and R. Sorrentino, "Conductor loss computation in multiconductor MIC's by transverse resonance technique and modified perturbational method," *IEEE Trans. Microwave and Guided Wave Lett.*, vol. 2, no. 6, pp. 250–252, June 1992.

[6] T. Kitazawa and T. Itoh, "Propagation characteristics of coplanar-type transmission lines with lossy media," *IEEE Trans. Microwave Theory Tech.*, vol. 39, no. 10, pp. 1694–1700, Oct. 1991.

[7] T. Kitazawa, D. Polifko, and H. Ogawa, "Analysis of CPW for LiNb optical modulator by extended spectral domain approach," *IEEE Microwave and Guided Wave Lett.*, vol. 2, no. 8, pp. 313–315, Aug. 1992.

[8] W. Heinrich, "Full-wave analysis of conductor losses on MMIC transmission lines," *IEEE Trans. Microwave Theory Tech.*, vol. 38, no. 10, pp. 1468–1472, Oct. 1990.

[9] C.-C. Tien, C. C. Tzuang, and S. T. Peng, "Effect of finite-width backside plane on overmoded conductor-backed coplanar waveguide," *IEEE Microwave and Guided Wave Lett.*, vol. 3, no. 8, pp. 259–261, Aug. 1993.

[10] K. Wu, R. Vahldieck, J. L. Fikart, and H. Minkus, "The influence of finite conductor thickness and conductivity on fundamental and higher-order modes in miniature hybrid MIC's (MHMIC's) and MMIC's," *IEEE Trans. Microwave Theory Tech.*, vol. 41, no. 3, pp. 421–430, Mar. 1993.

[11] S. A. Meade and C. J. Railton, "Efficient implementation of the spectral domain method including precalculated basis functions," in *1993 IEEE MTT-S Int. Microwave Symp. Dig.*, Atlanta, pp. 991–994.

[12] W. H. Haydl, "Experimentally observed frequency variation of the attenuation of millimeter-wave coplanar transmission lines with thin metallization," *IEEE Microwave and Guided Wave Lett.*, vol. 2, no. 8, pp. 322–324, Aug. 1992.

[13] Y. C. Shih and M. Maher, "Characterization of conductor-backed coplanar waveguides using accurate on-wafer measurement techniques," in *1990 IEEE MTT-S Int. Microwave Symp. Dig.*, Dallas, pp. 1129–1132.

[14] T. Itoh, *Numerical Techniques for Microwave and Millimeter-Wave Passive Structures.* New York: Wiley, 1989.

[15] N. K. Das and D. M. Pozar, "A generalized spectral-domain Green's function for multilayer dielectric substrates with application to multilayer transmission lines," *IEEE Trans. Microwave Theory Tech.*, vol. 35, no. 3, pp. 326-335, Mar. 1987.

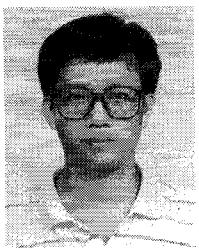

Jeng-Yi Ke was born in Taoyuan, Taiwan, R.O.C., on January 2, 1966. He received the B.S. degree in physics from National Taiwan Normal University, Taipei, Taiwan, in 1989, and the M.S.E.E. degree from National Taiwan University, Taipei, Taiwan in 1991. Since 1991 he has been working towards the Ph.D. degree in electrical engineering at National Taiwan University. His current research interests include analysis of planar transmission lines and leaky wave.

Chun Hsiung Chen was born in Taipei, Taiwan, R.O.C., on March 7, 1937. He received the B.S.E.E. degree from National Taiwan University, Taipei, Taiwan, in 1960, the M.S.E.E. degree from National Chiao Tung University, Hsinchu, Taiwan, in 1962, and the Ph.D. degree in electrical engineering from National Taiwan University in 1972.

In 1963, he joined the faculty of the Department of Electrical Engineering, National Taiwan University, where he is now a professor. From August 1982–July 1985 he was Chairman of the department. In 1974 he was a visiting researcher for one year in the Department of Electrical Engineering and Computer Sciences, University of California, Berkeley. From August 1986 to July 1987, he was a visiting professor in the Department of Electrical Engineering, University of Houston, Texas. In 1989 and 1990, he visited the Microwave Department, Technical University of Munich, Germany and Laboratoire d'Optique Electromagnetique, Faculte des Sciences et Techniques de Saint-Jerome, Universite d'Aix-Marseille III, France, respectively. His areas of interest include antenna and waveguide analysis, propagation and scattering of waves, and numerical techniques in electromagnetics.